*Chemometrics and Intelligent Laboratory Systems*, 14 (1992) 375–390
Elsevier Science Publishers B.V., Amsterdam

# Some special topics in multivariate image analysis

Paul Geladi

*Center for Peat Research, Box 4097, S 90403 Umeå, and Research Group for Chemometrics, University of Umeå, S 90187 Umeå (Sweden)*

(Received 19 July 1991; accepted 9 December 1991)

**Abstract**

Geladi, P., 1992. Some special topics in multivariate image analysis. *Chemometrics and Intelligent Laboratory Systems*, 14: 375–390.

Methods for multivariate image analysis are based on the definition of the multivariate image as a stack of congruent images collected for different variables (wavelengths). The article describes theories and three different types of examples for analysis when the images available are not congruent. This requires transformation to a common base used to construct a multivariate image. After that, a multivariate analysis can be carried out and the loading plots can be used for exploratory analysis and classification. Two new strategies are introduced: one for comparing within a set of noncongruent univariate images and one for comparing within a set of multivariate images.

## INTRODUCTION

Methods for the analysis of multivariate images are explained in refs. 1–13. The methods presented there allow exploratory analysis, classification and regression. The requirement for these methods is that a stack of congruent images is available: the multivariate image (MVI). The different planes in the stack are the features measured for the variables. A brief explanation of principal component analysis (PCA) on multivariate images is given in refs. 8–10, 12. It is sometimes necessary to deviate from the requirement of congruence in the stack. In these cases it is necessary to find some common base for the images. Theory and examples are given for three situations. The theory part presents descriptions of the methods and strategies used and some possible extensions. The emphasis is on the use of loading plots. The examples are of an illustrative nature and do not represent all aspects of the theory. They give good indications of what is possible. The methods proposed allow a huge number of modifications which can be introduced in a problem-dependent context. Not all of these modifications are explored in this paper, but some of them are indicated.

The first situation is that where a stack of images of varying degrees of defocusing is collected with the goal of finding the image of best focus. Two examples are given: one from microscopy and one from macroscopy. It is shown that focusing distance can be used as a pseudovariable in the multivariate image and that the loading plots give meaningful information on image quality. The images themselves can be re-

placed by their discrete two-dimensional Fourier transform (2D-FT) magnitude images to give slightly better results.

The second case is where a number of univariate (intensity, grey level) images have to be compared. This requires transformation to a common base for being able to construct a multivariate image. In this case the two-dimensional discrete Fourier transform is used to create a common base and the multivariate image consists of the magnitude spectra. The example given is from size and shape studies of wood chips used as a solid fuel. The strategy presented is called ASUNIM: analysis of a set of univariate images.

The third case is the comparison of a number of noncongruent multivariate images. These are brought to a common base by carrying out principal component analysis and drawing the score plots. The score plots are on a common base and are very specific for the multivariate images that they represent. The example is a constructed chemical example of different mixtures. The image material consists of subsamples of a larger image. For the sake of the argument, the information in the larger image is ignored. The strategy presented is called ASMULIM: analysis of a set of multivariate images.

In all three cases multivariate image analysis is possible and the loading plots are useful for carrying out exploratory analysis and classification of the entities (univariate and multivariate images) under study.

### *General technical details*

Images were collected using a variety of camera and illumination systems. The common technical features are described in this section, in order to avoid repetition. Specific equipment and methods used are mentioned under each experiment heading. Digitizing was done with Kontron's IBAS hardware and Version 2.0 software on a 386/387 host PC. All images were digitized in the intensity range 0–255, often in size $512 \times 512$. Also discrete two-dimensional Fourier transform and other filtering and contrast stretching operations were carried out on the IBAS equipment. Multivariate image analysis (MIA) was done on a 386/387 PC in the ERDAS [14] environment, using the Revolution Number Nine image display board and a multisync monitor. The functions of MIA [9] and other ERDAS modules were used. Some of the MIA functions were modified especially for the experiments described in this paper. All photographs were taken from a multisync screen on black and white negative (100 ISO) or color positive (200 ISO) film. Some geometrical deformation of resulting images may have occurred.

## MULTIVARIATE IMAGE ANALYSIS BY PRINCIPAL COMPONENT ANALYSIS

A multivariate image is a stack of congruent images of the same scene or object, each measured for a different variable (e.g. wavelength) [1,2]. Combined with the often rectangular geometrical shape of a digitized image, this gives a three-way array of size 'number of variables' × 'number of columns' × 'number of rows'. A typical size is $Q$ variables × 512 columns × 512 rows. An illustration is shown in Fig. 1. All the multivariate methods available in chemometrics can in principle be applied to a multivariate image. A useful simplification is that the multivariate image can be seen as a data matrix with $512 \times 512$ objects (262 144 objects) and $Q$ variables. This is very convenient for calculations e.g. principal component analysis [8–10,12,13] and latent variable regression [11,15]. The advantage of using images is that the geometrical relationship also exists after the calculations, so that latent variable images can be constructed. These latent variable images are ideal for an interactive visual interpretation of the data.

The multivariate method used in this paper is principal component analysis (PCA). Fig. 1 shows the principles of the method. Sometimes the data are preprocessed. Mean-centering, variable-wise linear rescaling (such as stretching) and nonlinear rescaling (such as taking the logarithm) can be applied before the principal component model is calculated. Contextual operations (linear and nonlinear neighbourhood operations) on the raw images can also be applied [16]. The method of

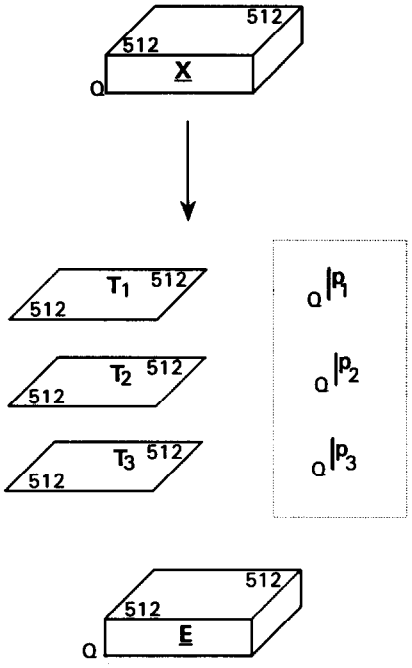


Fig. 1. A multivariate image of size e.g. $Q$ variables and $512 \times 512$ can be decomposed into loading vectors (size $Q$), score matrices (only three shown here), and a residual array of size $Q \times 512 \times 512$. In this paper, the emphasis is on the loading vectors.

preprocessing used will be explained separately for each example. A data array $\underline{\mathbf{X}}$ is decomposed in a sum of three-way products * of score images $\mathbf{T}_a$ and loading vectors $\boldsymbol{p}_a$ and a residual $\underline{\mathbf{E}}$:

$$\underline{\mathbf{X}} = \sum_{a=1}^{A} \mathbf{T}_a * \boldsymbol{p}_a + \underline{\mathbf{E}}$$

The matrices $\mathbf{T}_a$ have the same geometrical organization as the raw images and are used as score images. Looking at score images can be informative, but is very subjective. A more objective way to study the variable space of a multivariate image is to study the scatter plots of the score images. This has been presented in earlier publications [8–10,12,13]. The examples presented here make use of the loading vectors and loading plots. Loadings are weight factors for combining the raw images into score images. Small loading values for a variable mean that the contribution to the principal component model is small. Proximity in the loading plots means that two variables contribute in a similar way to the principal component model.

## SELECTION OF BEST FOCUS

In many situations in automated image analysis it is necessary to select a best focused image from a number of more or less defocused images of the same object or scene. Many assumptions can be made regarding the way to describe the concept of 'in focus'. The method presented does not make use of these kinds of assumptions. It is a soft modeling approach, where the structure in the data themselves is used in a multivariate way. The images of different focus are collected in a stack, a multivariate image. This is shown schematically in Fig. 2. This has been done for two examples: one from a microscopic study and one from a macroscopic study. The hypothetical situation is that of a machine trying to detect the point of optimal focus, without human intervention. The strategy is simply called 'focus'.

The microscopic image is a sample from the botanical studies of peat. Image collection was done in a Zeiss Universal microscope with a 3.2× objective. The TV camera used was a DAGE-MTI CCD 72. The images were taken by 10× averaging for noise reduction. Eight images

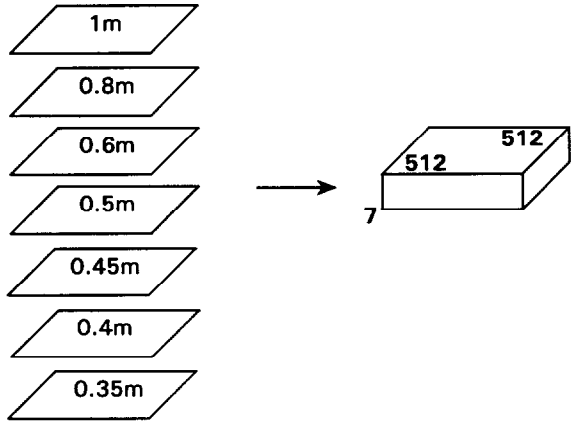


Fig. 2. The seven images taken with different focus (as read from the focusing ring of the objective) are combined into a seven-variable multivariate image. The array has a size of $7 \times 512 \times 512$.

of different focus of size 512 × 512 were collected by increasing the distance between objective and sample. They represent a sphagnum (white moss) leaf. The total image size is about 0.85 mm × 0.85 mm. The images are shown in Fig. 3. Subjectively, image number 4 seems to be the best focused, with numbers 3 and 5 as next best choices. Fig. 4 shows the two-dimensional discrete Fourier transform magnitude images of the eight images in Fig. 3.

The macroscopic image is from studies of solid fuel. The image is of wood and bark chips on a background of white paper. The seven 512 × 512 images were taken with a DAGE-MTI camera using a P8029 25.4 mm diameter PbS tube. Illumination was with a quartz-halogen projection lamp in a Schott KL1500 lamp house, going out into two 4-mm diameter glass fibre cables towards the sample. The objective used was a Pentax 50 mm MACRO/*f* 2.8. Digitization was carried out with 10 × averaging to reduce random noise. The field shown in Fig. 5 is approximately 5 cm × 5 cm. Subjectively, image 5 seems to be the one with the best focus.

The image was analyzed in two ways. First the multivariate image of the images of different focus was analyzed by PCA, without mean-centering or rescaling. The second way is by first taking the discrete two-dimensional Fourier transform and making a multivariate image of the magnitude spectra. A description of the discrete two-dimensional fast Fourier transform (2D-FFT) is given in an Appendix. A 512 × 512 image gives a 512 × 256 magnitude spectrum. Also the multivariate image of size $Q \times 512 \times 256$ can be decomposed by PCA. The results of the PCA analysis are shown in Table 1 for the microscopic example and in Table 2 for the macroscopic example. In both cases the thing to study is the loading plot. The loadings for the first component showed nothing special. The loading plots for components 2 and 3 are very useful. They are shown in Fig. 6.

For the raw images, in both Tables 1 and 2, the first principal component (PC) describes the major part of the total sum of squares. This first PC only describes the average intensity and does not contain much information on the differences between images in the stack. The further PCs decrease quickly in size. For the 2D-FT magnitude images, the first component describes less of the total sum of squares than for the raw images.

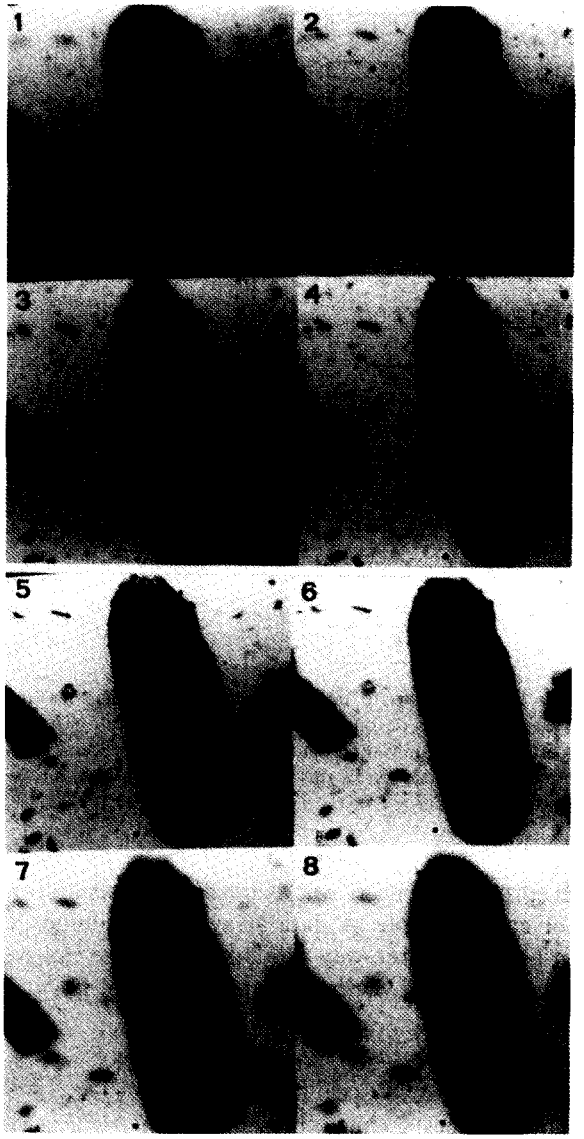


Fig. 3. The 'focus' experiment. The microscopic image is a sample from the botanical study of peat. It represents a sphagnum (white moss) leaf and other botanical residues. The total sampled image size is about 0.85 mm × 0.85 mm. Eight images of different focus, each of size 512 × 512 were collected by increasing the distance between objective and sample. Subjectively, image number 4 seems to be the best focused, with numbers 3 and 5 as next best choices.

The information is also more spread out over the following components.

A study of the loading plots in Fig. 6 shows some very interesting points. In all four loading plots it seems that the second principal component separates the well-focused images from those with bad focus. An increased value for the second loading is interpreted as 'better focus'. For the 2D-FT this is even more pronounced than for the raw images. The third PC gives a separation into 'below focus' and 'above focus', so that, in combination with PC2, there is a circular pattern describing the sequence in which the images were taken. This is an interesting property that cannot be inferred by visual inspection of the raw images in Figs. 3 and 5.

## CLASSIFICATION OF UNIVARIATE IMAGES. THE ASUNIM STRATEGY

In some cases it is necessary to compare univariate images of different content. Many transformations and calculations can be used for this goal. Images of different objects or scenes cannot be used directly to build up a multivariate image, because of the lack of congruence. It is necessary to find a common base on which to construct a multivariate image. Many methods exist for constructing orthogonal bases for representing im-

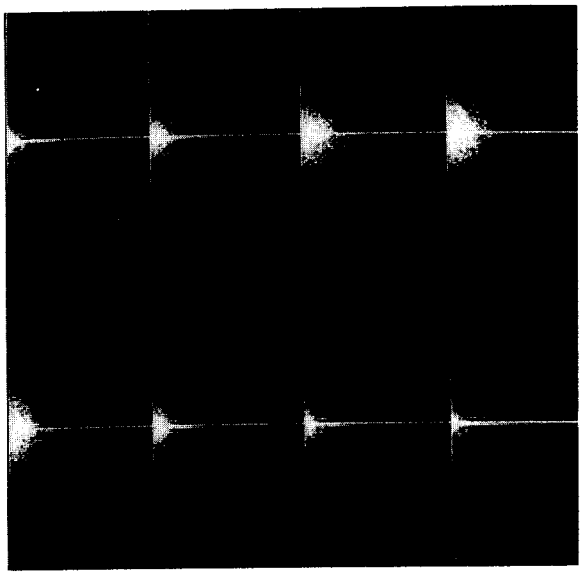

Fig. 4. The 'focus' experiment. The discrete two-dimensional Fourier transform magnitude images of the eight images of Fig. 3. Top row, left to right: the magnitude images of images 1–4. Bottom row, left to right: the magnitude images of images 5–8. The magnitude images have size 512×256. Because of the symmetry of the magnitude function half of the 512×512 magnitude image can be omitted.

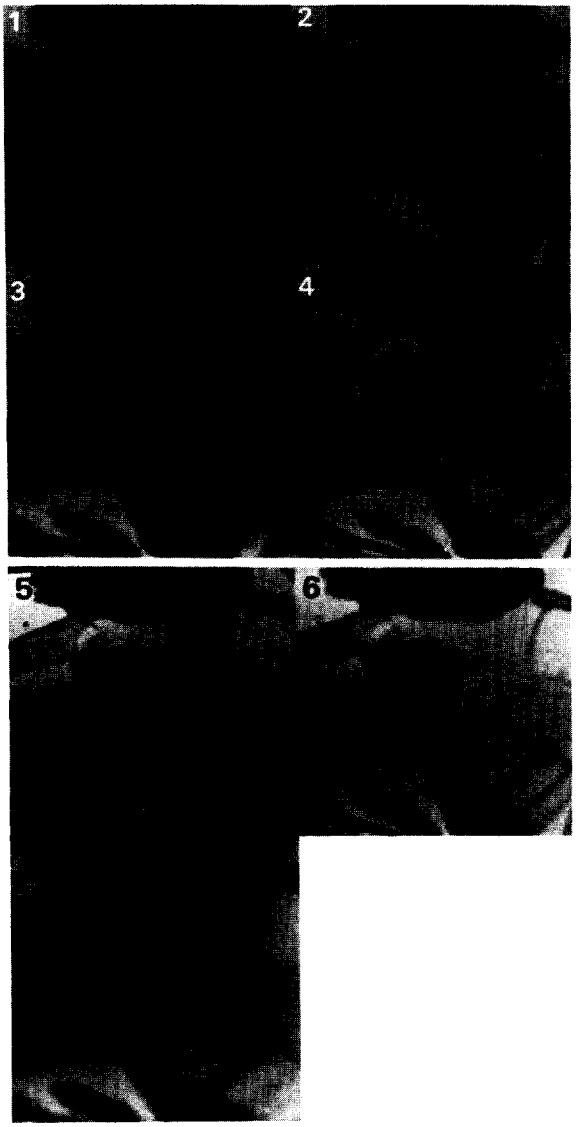


Fig. 5. The 'focus' experiment. The macroscopic image is from a study of solid fuel, showing wood and bark chips on a background of white paper. The scene shown has approximate size 5 cm×5 cm. Image 5 seems to posses the best focus when subjective visual inspection is performed.

TABLE 1

Results of the PCA analysis for the microscopic 'focus' experiment

| Component No. | SS raw * (%) | SS 2D-FFT * (%) |
|---|---|---|
| 1 | 99.67 | 86.72 |
| 2 | 0.17 | 3.5 |
| 3 | 0.12 | 2.0 |
| 4 | 0.025 | 1.7 |
| 5 | 0.011 | 1.6 |
| 6 | 0.003 | 1.5 |
| 7 | 0.0009 | 1.5 |
| 8 | 0.0004 | 1.4 |

* SS = sum of squares.

TABLE 2

Results of the PCA analysis for the macroscopic 'focus' experiment

| Component No. | SS raw (%) | SS 2D-FFT (%) |
|---|---|---|
| 1 | 99.24 | 80.6 |
| 2 | 0.39 | 4.5 |
| 3 | 0.19 | 3.2 |
| 4 | 0.10 | 3.2 |
| 5 | 0.04 | 3.0 |
| 6 | 0.03 | 2.9 |
| 7 | 0.01 | 2.7 |

ages and other two-dimensional arrays [17,18]. One of the more useful ones is the Fourier transform (see the Appendix, also previous section). The discrete two-dimensional fast Fourier transform allows the construction of a magnitude image from the original image.

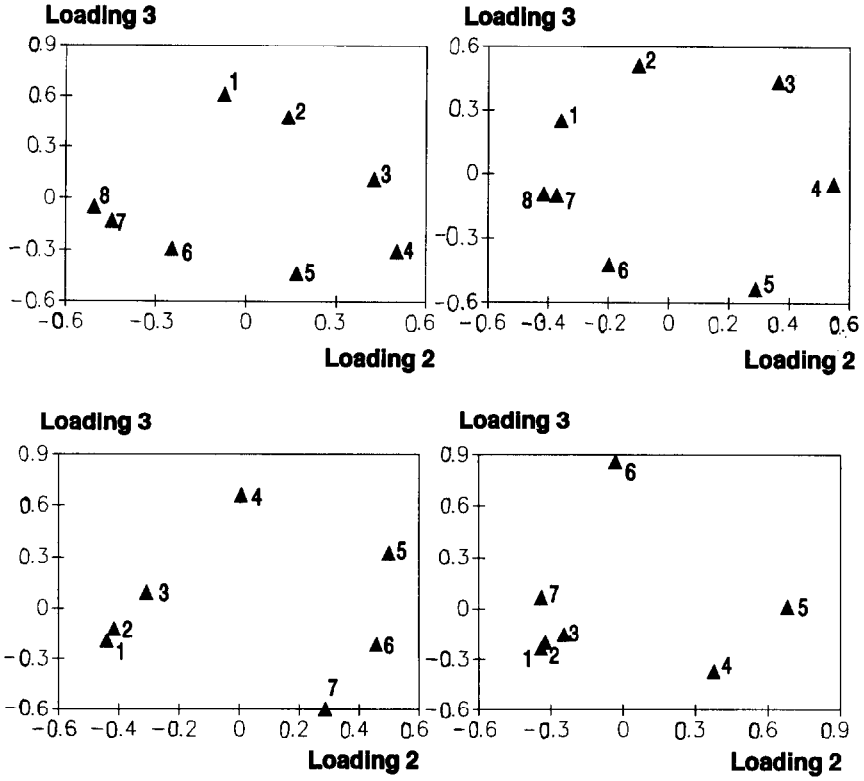


Fig. 6. Results of the 'focus' experiment. The loading plots for components 2 (horizontal axis) and 3 (vertical axis). Upper plots are for the microscopic experiment, lower plots are for the macroscopic experiment. Left plots are for the raw image data and right plots are for the discrete 2D-FFT. Note that the plots have different scales. The plots show images of best focus to the right and of worst focus to the left. The reader may also note that above and below focus images are separated.

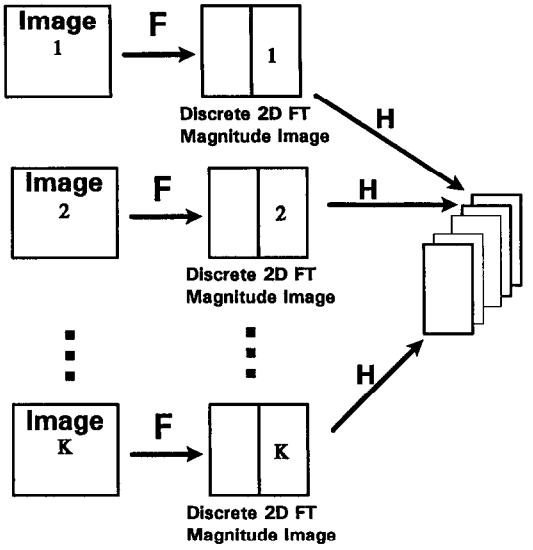


Fig. 7. The ASUNIM strategy. A set of $K$ intensity (univariate) images can be transformed by the function **F** into a set of $K$ discrete two-dimensional Fourier transform magnitude images. Because of the symmetry of the magnitude function only half the magnitude image is used. The halves are used to form a multivariate image. Before forming the multivariate image, a function **H** can be applied to the magnitude images. This function **H** can be any function deemed useful for the purpose of improving the subsequent analysis of the multivariate image.

The ASUNIM strategy is explained in Fig. 7, which shows how $K$ univariate (intensity) images in a set have to be compared. After transformation to magnitude spectra, the images are on a common base and can be used to build a multivariate image. It should be mentioned here that, in order to be comparable after transformation to a common base, all the images should be collected in a reproducible way in the same physical environment (illumination, camera etc.). Principal component analysis allows projection from multivariate space into loading plots. The loading plots are used for exploratory analysis and classification in the original set of $K$ images. Instead of the magnitude image, the separate real and imaginary data sets could be used, but they are not in image form and the floating point format that they are in makes calculations more cumbersome.

The example is from energy research. Wood chips used as a solid fuel are studied. The example is shown in Fig. 8. The thirteen intensity images represent the following classes: (a) small rectangular particles, (b) large rectangular particles, and (c) long particles. The images were collected with a DAGE-MTI CCD 72 camera using a Pentax 50 mm MACRO $f/2.8$ objective. Illumination was with fluorescent tubes. The sampled area is approximately 8 cm $\times$ 8 cm. Digitization was done with 10 $\times$ averaging to reduce random noise. The images were collected as 512 $\times$ 512 images. The wood chips were spread out with random positions and random orientation. Discrete two-dimensional fast Fourier transformation was performed, leading to magnitude images (see Appendix). Because of the symmetry of the magnitude function, only half of the magnitude image is used. A multivariate image of size $13 \times 512 \times 256$ was constructed. The thirteen individual magnitude images are shown in Fig. 9. Even though Fig. 9 displays differences between the magnitude images, it is difficult to give an

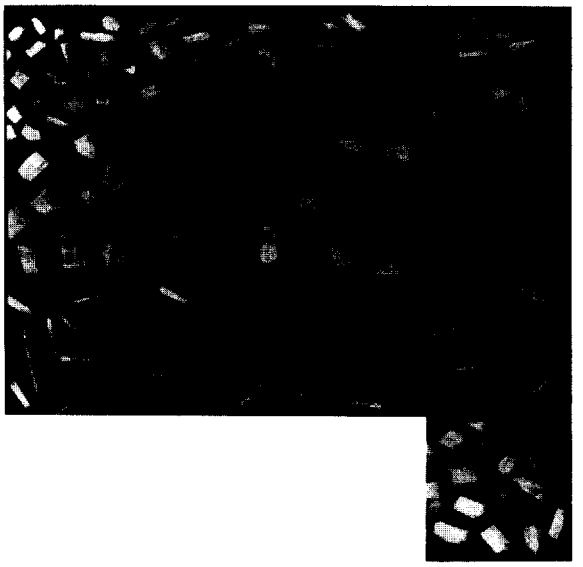

Fig. 8. The ASUNIM experiment. This example is from energy research. Wood chips used as a solid fuel are studied. The thirteen intensity images of size 512×512 represent the following classes: (a) small 'rectangular' particles (first row: left to right, images 1–4); (b) large 'rectangular' particles (second row: left to right, images 5–8); and (c) long particles (third row: left to right, images 9–12). Image 13 is on row 4 and represents something between class a and class b, but probably closer to class a.

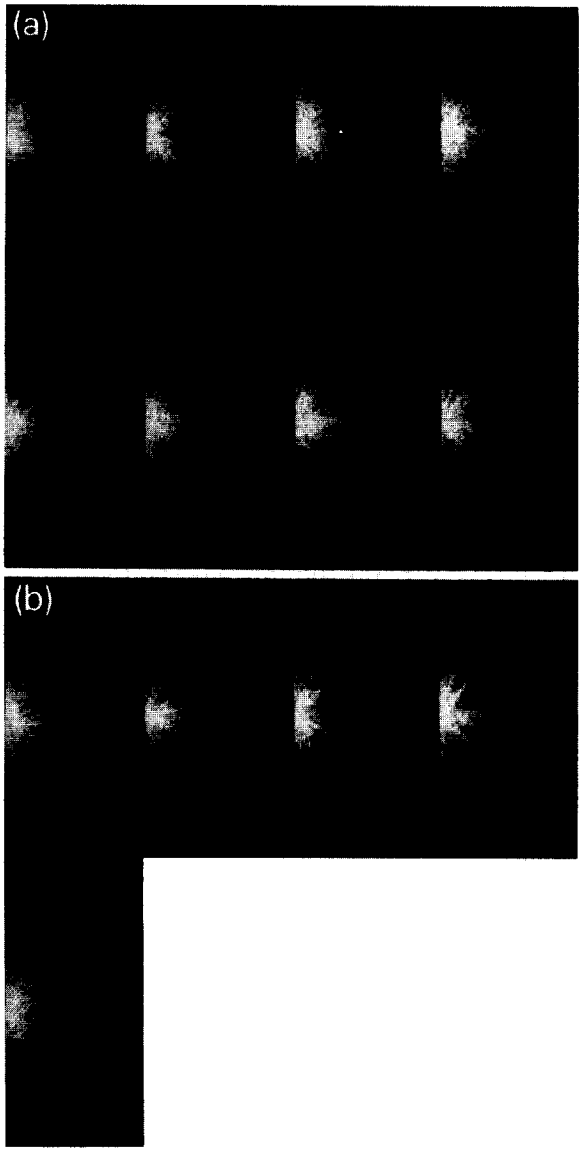


Fig. 9. The ASUNIM experiment. The thirteen magnitude images of the images in Fig. 8. (a) Top row, left to right, images 1–4; bottom row, left to right, images 5–8. (b) Top row, left to right, images 9–12; bottom row, image 13. Because of the symmetry of the magnitude function these images are only of size 512×256.

objective description of the relationships between the original intensity images. One observation that can be made is that high spatial frequencies probably do not contribute too much to the information in the magnitude images and therefore can be left out. An MVI of size 13 × 100 × 50 was constructed by removing the high-frequency coefficients from the magnitude spectra.

Principal component analysis was caried out on the 13 × 512 × 256 MVI (all frequencies) and the 13 × 100 × 50 MVI (low frequencies), without rescaling, but with variable-wise mean subtraction. Some of the results of this analysis are shown in Table 3.

The important aspect of this analysis is the study of the loading plots, showing the relationships between the univariate images. The first component loadings showed nothing interesting. Fig. 10 shows the loading plots for the ASUNIM example, using loadings for components 2, 3 and 4 for the 'all frequencies' and the 'low frequencies' cases. Classes a (members 1–4) and b (members 5–8) are well separated in the 2–3 loading plots, and not so well separated in the 2–4 loading plots. The members of class c (9–12) occupy extreme positions in the plots. The images 9–12 also have the greatest statistical variability. Image 13, containing elements from classes a and b, is classified closer to class a. The 'low frequencies' case shows slightly less separation of classes, but still a reasonable one.

Other operations could have been carried out to improve the results. It is possible to filter, rescale or smooth the magnitude images before PCA analysis (function **H** in Fig. 7). There are also many ways of selecting 'useful' spatial frequencies of the magnitude images. Bearing these facts in mind, the method looks very promising. The two-dimensional Fourier transform also has some limitations. The magnitude image is sensi-

TABLE 3

The ASUNIM experiment. Results of the PCA on the 13×512×256 (all frequencies) and 13×100×50 (low frequencies) MVIs

| Component | % SS explained for frequencies | |
|---|---|---|
| | All | Low |
| 1 | 88.4 | 95.6 |
| 2 | 1.5 | 0.71 |
| 3 | 1.4 | 0.50 |
| 4 | 1.3 | 0.47 |
| 5 | 1.3 | 0.44 |

tive to the shape of a single particle and to orientation of the particles. The strategy only works for a statistical significant number of particles spread out in random orientation. In industry and research this kind of problem is often encountered in the study of powders and particles.

## CLASSIFICATION OF MULTIVARIATE IMAGES. THE ASMULIM STRATEGY

Multivariate images contain more information than univariate ones. Therefore it is necessary to have a method of comparing noncongruent multivariate images. A set of K multivariate images is given (Fig. 11) and it is necessary to establish relationships between them. Many properties may be extracted from a multivariate image to make classification or discrimination inside the set possible. The way this is done is problem-dependent. Sometimes assumptions have to be made about the relation of the multivariate image to the problem at hand. The approach presented here is one in which assumptions are avoided as far as possible.

The set of multivariate images is transformed into a new MVI, where each member of the set is a plane in the new MVI. This means that there must be a congruent common base. It was shown earlier that the score plots provide very specific

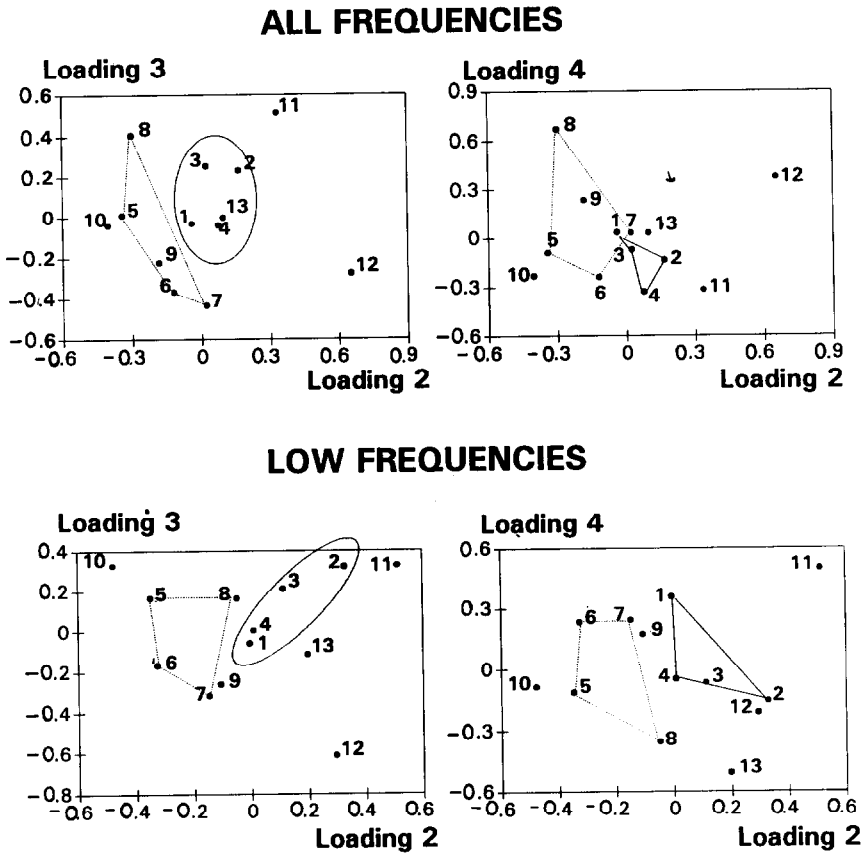


Fig. 10. The loading plots for the ASUNIM strategy applied to the example, using loadings for components 2, 3 and 4 for the 'all frequencies' and the 'low frequencies' cases. Classes a (members 1–4) and b (members 5–8) are well separated in the 2–3 loading plots, and not so well separated in the 2–4 loading plots. The members of class c (9–12) occupy extreme positions in the plots. The images 9–12 also have the greatest statistical variability. Image 13, containing elements from classes a and b, is classified closer to class a. Note that the plots have different scales.

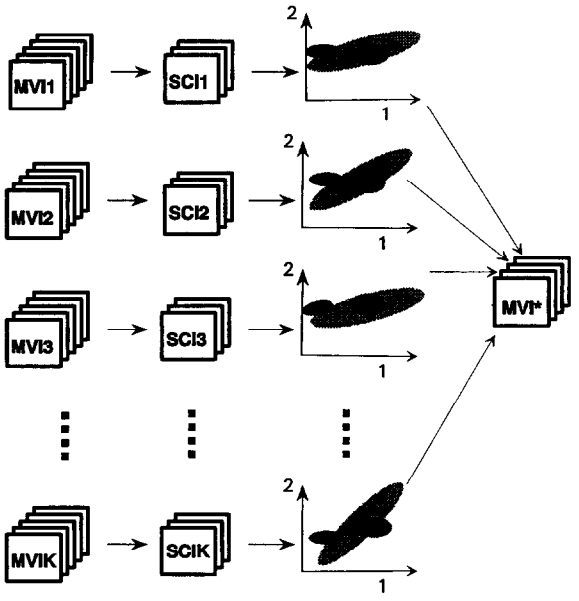


Fig. 11. The ASMULIM strategy. When $K$ multivariate images (MVI1 to MVI$K$, for an example see Fig. 13) have to be brought to a common base, it is possible to calculate their score images (SCI1 to SCI$K$). The score plots constructed from these images are on a common base and can be compared (for an example see Fig. 14). Since the score plots can be treated as images themselves, it is possible to construct the multivariate image MVI* with them. MVI* has $K$ planes representing the $K$ original multivariate images.

ways of observing properties of multivariate images. Things like dense classes, outliers and gradients can be detected there. When calculated in the right fashion, score plots can also form a common base for describing the content and properties of multivariate images.

Fig. 11 gives an outline of the strategy of ASMULIM. The $K$ multivariate images (of $Q$ variables each) in the set are each subjected to a PCA analysis, leading to $K$ stacks of score images. Score plots are constructed from these score images. These score plots themselves can be treated as images and, provided that the calculations were done in the right way, they are on a common base. This allows the creation of a new multivariate image of $K$ variables: In MVI*, each plane in the stack is a representative of one MVI in the set of $K$. Fig. 12 shows how a further PCA analysis on MVI* leads to loading plots showing the relationships between the $K$ planes

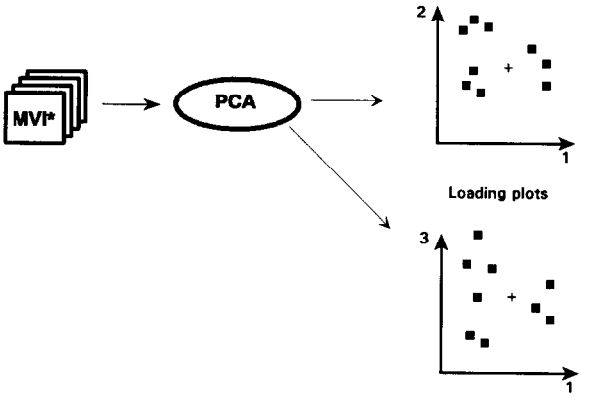


Fig. 12. The multivariate image MVI* can be subjected to PCA analysis. The loading plots allow exploratory analysis and classification. The points in the loading plots refer to the $K$ MVIs in the original set of Fig. 11.

and therefore relationships between the $K$ multivariate images of the set. The method introduced here is very flexible and extensions are presented further on in the text.

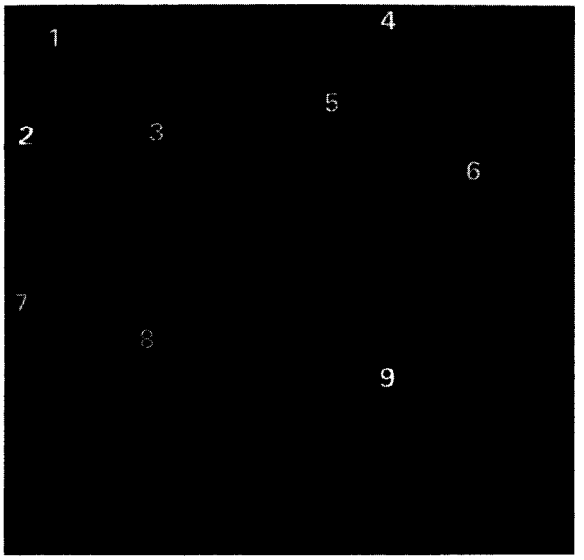


Fig. 13. The ASMULIM experiment. A set of nine ($K = 9$) multivariate images of size 64×64 were sampled from a 512×512 multivariate image of nine variables ($Q = 9$). The variables are the wavelengths: 1210, 900, 840, 800, 740, 680, 630, 580 and 540 nm. The total 512×512 image size is approximately 4 cm×4 cm. The four mixtures in the four quadrants are described in the text.

The example is shown in Fig. 13. It is an image of four mixtures on a dark background. The mixtures are: (a) upper left corner NaCl coarse crystals 100%; (b) upper right corner 50% w/w NaCl + 50% w/w sugar, fine ground; (c) lower left corner 50% w/w sugar + 50% w/w NaCl coarse crystals; and (d) lower right corner 100% sugar, coarse crystals. The image was collected at nine wavelengths, given below Fig. 13 and of size 512 × 512. The experimental technique used is described in ref. 13. From the nine-variable image, nine different 64 × 64 subsamples were selected to give a set of nine different multivariate images. The location of the samples is given in Fig. 13. For the sake of argument, it should be assumed that the large 512 × 512 image does not exist and that the subsamples are only available as separate images. A complete analysis of the large image is described in refs. 16 and 19. The subsamples were chosen to belong to the classes of mixtures as follows: three subsamples from mixture a, three subsamples from mixture b, and two and one subsamples from mixtures c and d, respectively. PCA was carried out on these images without rescaling or mean-centering and the score images were calculated. The 1–2 score images of size 256 × 256 are shown in Fig. 14. These score images are on a common base and a multivariate image can be built up from them, as shown in Fig. 11. This multivariate image can then in its turn be subjected to PCA analysis. The PCA analysis was carried out without rescaling or mean-centering. The results of this analysis are shown in Table 4. From this table it is expected that the components 1–3 explain the most important phenomena. The loading plots resulting from this analysis are shown in Fig. 15. These loading plots are projections from the object space of MVI*. The loading plots of the analysis are able to separate classes and show outliers in a very distinctive manner. This is explained below Fig. 15.

Further developments of the technique are possible. More than one score plot can be used, and three-way score plots could even be constructed. See Fig. 16, where this is shown schematically. Also, the construction of the MVI* can be associated with pretreatment of the score-plot images, using the function **H**. There could be smoothing, edge detection, low- and high-pass filtering etc. This is shown in Fig. 17.

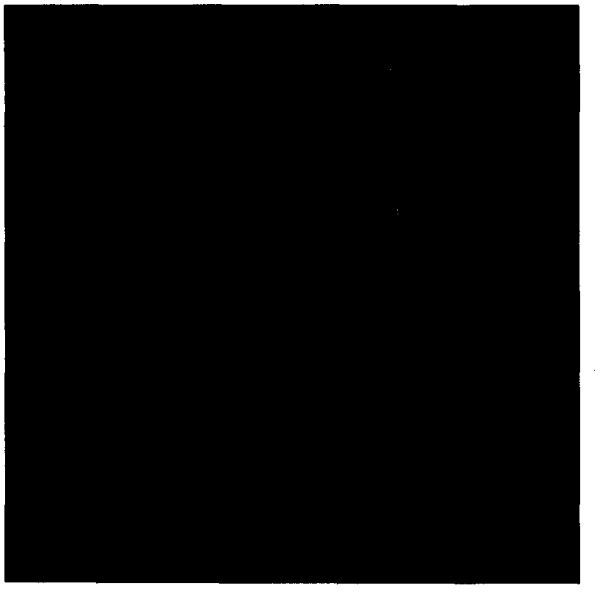

Fig. 14. The ASMULIM experiment. The score plots for components 1 (horizontal) and 2 (vertical) for the nine 64 × 64 multivariate images are shown together in this picture (top row, left to right: 1–3; middle row, left to right: 4–6; bottom row, left to right: 7–9). Although some differences can be observed, it is difficult to make an objective classification based on them.

## CONCLUSION

A multivariate soft modeling is possible, even in the case of noncongruent images, using the techniques from multivariate image analysis. The main property of the methods explained is the transformation to a common base. Except for this operation, no assumptions have to be made. The structure of the constructed multivariate space shows itself in the loading plots. The classifications presented were of an exploratory nature, but further developments will lead to possible unsupervised and supervised classification. This may become extremely useful for industrial inspection, for example.

The 'focus' examples are successful applications and a good illustration of the principles

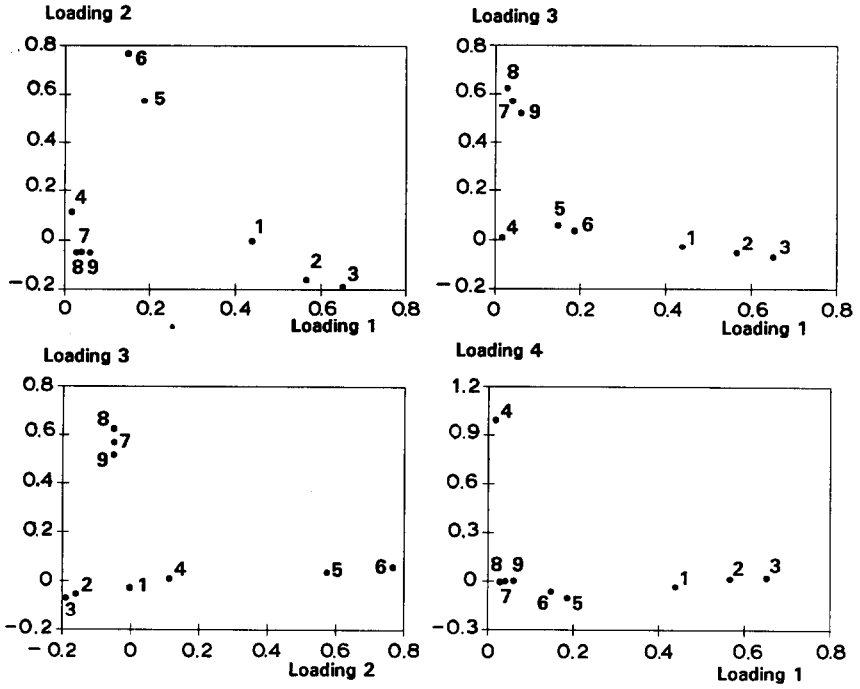


Fig. 15. The results of the ASMULIM experiment for the provided example. Loading plots for the example show the following: MVIs 7, 8 and 9 are very similar and cannot be separated. MVI 4 is an outlier, as seen in the 1–4 loading plot. Three classes of MVIs can be separated, as seen in the 1–3 loading plot. Note that the plots have different scales.

involved in the method for finding the image of best focus without human interaction. Whether they are of any other than didactical use will have to be found out in the future.

The exploratory analysis and classification of a set of $K$ univariate (intensity) images works well after transformation to a common base, as shown

TABLE 4

The ASMULIM experiment. Results of the PCA analysis, percentage of sum of squares (SS) explained per component

| Component | SS explained (%) | |
|---|---|---|
| | Per component | Cumulative |
| 1 | 32.0 | 32.0 |
| 2 | 21.8 | 53.8 |
| 3 | 20.6 | 74.4 |
| 4 | 8.6 | 83.0 |
| 5 | 5.3 | 88.3 |

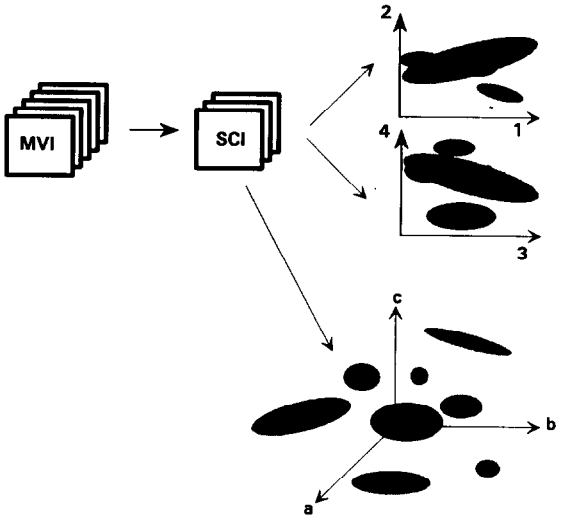


Fig. 16. The ASMULIM strategy presented in Figs. 11 and 12 can be amended by the use of more than one two-dimensional score plot, or even three-dimensional score plots.

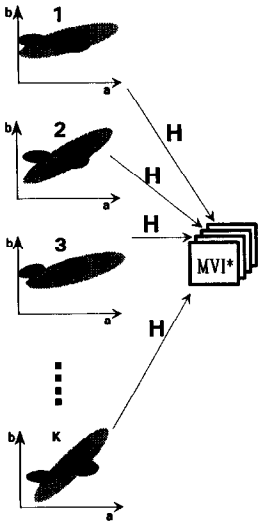


Fig. 17. The score plots of Figs. 11 and 12 can be transformed by applying a function **H** before MVI* is built. The function can be a smoothing, edge detection, low-pass filtering, etc.

in the ASUNIM example. The common base is the magnitude image obtained after discrete two-dimensional (fast) Fourier transformation. In order to achieve comparability, the experimental conditions for obtaining the $K$ intensity images in the set should be kept constant. There is also a limitation on the objects or scenes studied. Each scene should have a statistically significant number of particles in a random orientation. There are many occasions in research, technology and industry where such images occur. Particle size and shape analysis are common applications of image analysis.

The example of exploratory analysis and classification in a set of $K$ multivariate images (ASMULIM) shown, together with the example provided, gives very good results. Here, too, the experimental conditions of image collection, including the choice of variables, should be kept constant in order to maintain comparability. Together with the possible extensions this may turn out to become a powerful method for industrial inspection, quality control and similar applications. It would be possible to make a dense class representing the 'normal' image in the loading plot, and to project further images in the same space for comparison and detection of outliers.

In order to make the presented methods and strategies useful, the theories should be tested in greater detail and with more extensions, and more examples should be analyzed.

ACKNOWLEDGEMENTS

Helén Bergner, of the Center for Peat Research, is thanked for technical assistance in sample preparation. Christer Albano, of the Center for Peat Research and Fredrik Lindgren of the University of Umeå are thanked for interesting discussions and proofreading.

## APPENDIX. THE DISCRETE TWO-DIMENSIONAL FOURIER TRANSFORM FOR IMAGES

The Fourier transform is used for transforming data or functions from the time domain to the spectral domain, or in general from one domain to another. For example, a sound wave from a musical instrument as shown on an oscilloscope screen represents an intensity varying as a function of time. The Fourier transform of this sound wave is a representation of the frequencies present in it, where each frequency has an associated amplitude. The former representation as a time-dependent function is the way electronic amplifiers are supposed to treat the electrical signal. The latter representation as a frequency spectrum is the way the human ear perceives the sound. In the cases described in this paper, the transform is from the spatial domain to the spatial frequency domain. The one-dimensional Fourier transform has been treated extensively in chemistry. The basic principles of one-dimensional Fourier transform are explained in refs. 20–22.

The two-dimensional Fourier transform is explained in refs. 17, 23, and 24. The notation of ref. 17 is used. The two-dimensional Fourier transform is given for a continuous two-dimensional function $f(x, y)$:

$$\mathcal{F}(w_x, w_y) = \int_{-\infty}^{\infty}\int_{-\infty}^{\infty} f(x, y) \times \exp\left[-i2\pi(w_x x + w_y y)\right] \mathrm{d}x\, \mathrm{d}y \quad \text{(A1)}$$

where $x$, $y$ are continuous spatial variables, $f(x, y)$ is a function of $x$ and $y$, $w_x$, $w_y$ are spatial frequencies in the $x$ and $y$ directions. Sometimes $2\pi$ is omitted from the equation and $w_x$ and $w_y$ are rescaled by a factor $2\pi$. $\mathcal{F}(w_x, w_y)$ is the two-dimensional Fourier transform.

The extension to Fourier transforms on three- and four-dimensional functions is easy. Eqn. A1 can also be expressed in composite ways, first as real and imaginary parts:

$$\mathcal{F}(w_x, w_y) = \mathcal{R}(w_x, w_y) + i\mathcal{I}(w_x, w_y) \quad \text{(A2)}$$

where $\mathcal{R}(w_x, w_y)$ is the real part of the two-dimensional Fourier transform, and $\mathcal{I}(w_x, w_y)$ is the imaginary part of the two-dimensional Fourier transform.

The other representation is in magnitude and phase parts:

$$\mathcal{F}(w_x, w_y) = \mathcal{M}(w_x, w_y) \exp\left[i\mathcal{T}(w_x, w_y)\right] \quad \text{(A3)}$$

where $\mathcal{M}(w_x, w_y)$ is the magnitude part of the two-dimensional Fourier transform, and $\mathcal{T}(w_x, w_y)$ is the phase part of the two-dimensional Fourier transform. Here

$$\mathcal{M}(w_x, w_y) = \left[\mathcal{R}^2(w_x, w_y) + \mathcal{I}^2(w_x, w_y)\right]^{1/2} \quad \text{(A4)}$$

$$\mathcal{T}(w_x, w_y) = \tan^{-1}\left[\mathcal{I}(w_x, w_y)/\mathcal{R}(w_x, w_y)\right] \quad \text{(A5)}$$

For real data, only discrete sampling points are used to make an image of $L \times N$ pixels. The following changes take place: (i) $f(x, y)$ is replaced by $f(l, n)$ $l = 1, \ldots, L$ $n = 1, \ldots, N$; (ii) the double integral is replaced by a double summation; (iii) the frequencies $w_x$ and $w_y$ are replaced by discrete spatial frequencies $w_l = 0, \ldots, L-1$ and $w_n = 0, \ldots, N-1$.

The discrete two-dimensional Fourier transform then looks like:

$$F(w_l, w_n) = \sum_{l=0}^{L-1} \sum_{n=0}^{N-1} f(l, n) \times \exp\left[-i2\pi(w_l l/L + w_n n/N)\right] \quad \text{(A6)}$$

When the number of sampling points $L$ and $N$ are powers of 2, the fast Fourier transform [17] can be used. Here, too, a composite representation into real and imaginary parts is possible:

$$F(w_l, w_n) = R(w_l, w_n) + iI(w_l, w_n) \quad \text{(A7)}$$

And a magnitude can be expressed:

$$M(w_l, w_n) = \left[R^2(w_l, w_n) + I^2(w_l, w_n)\right]^{1/2} \quad \text{(A8)}$$

This magnitude can be expressed as an image of size $N \times L$ where the size of $M$ is the intensity in the image. A special transformation is used to improve the subjective visual representation:

$$m(w_l, w_n) = k \ln\left[1 + \left[R^2(w_l, w_n) + I^2(w_l, w_n)\right]^{1/2}\right] \quad \text{(A9)}$$

where $m(w_l, w_n)$ is the intensity (magnitude) function represented in the image plane. There is also a truncation to integers. $k$ is a scaling coefficient, used to make the magnitude spectrum fill the whole range of grey values 0–255. ln is the base 2 logarithm. $R(w_l, w_n)$ is the real part of the discrete 2D-FT. $I(w_l, w_n)$ is the imaginary part of the discrete 2D-FT.

Because of the periodicity properties of the Fourier transform, the magnitude function is usually shown with the zero spatial frequencies in the middle of the image. Because of the absence of the phase part $m(w_l, w_n)$ is symmetrical and the two halves of the image representation are identical:

$$m(w_l, w_n) = m(-w_l, -w_n) \quad \text{(A10)}$$

The intensity function $m(w_l, w_n)$ shows which spatial frequencies are most abundant in the image. It can be used to select filter functions for high-pass and low-pass filtering.

An illustration is given in Fig. 18, in which the spatial images are shown on the left and the spatial frequency images on the right. In situation A, it is shown that the continuous variable $x$ is replaced by $l = 1, \ldots, L$ and the continuous variable $y$ is replaced by $n = 1, \ldots, N$. The magnitude image of Eqn. A9 is shifted, so the zeros are

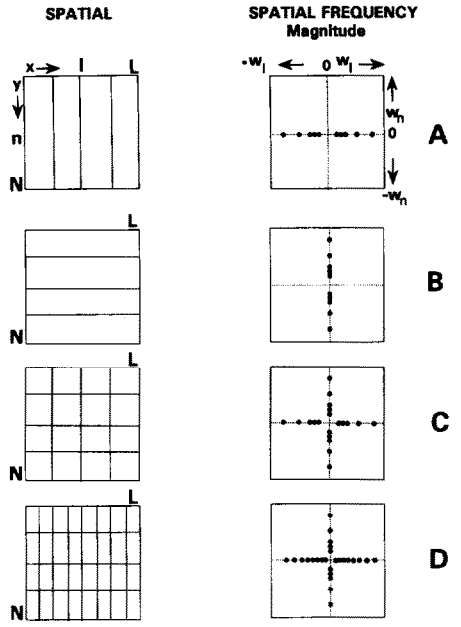


Fig. 18. A schematic overview of the properties of the discrete two-dimensional Fourier transform and its magnitude image. Situation A shows a univariate image of size $N$ lines and $L$ columns. Usually the image is square ($L = N$) and often $L$ and $N$ are powers of 2, allowing fast Fourier transform (FFT). The magnitude image to the left displays the magnitude function (Eqn. A9). The zero frequencies are in the middle. Further explanation may be found in the text.

in the middle of the image. The variables are $w_l$ and $w_n$. Because of the symmetry of the magnitude function (Eqn. A10), the left and right sides are identical and usually only the left or right side is used.

In situation A, the spatial image has vertical lines, giving variation in the horizontal direction, but no variation in the vertical direction. Therefore the magnitude function is zero, except for $w_n = 0$. If there had been a sinusoidally varying vertical pattern, the magnitude function would have been zero everywhere, except for one $w_l$ frequency. The square-wave pattern in situation A gives a number of harmonics, and so a number of values for $w_l$ are different from 0.

In situation B, the spatial image has horizontal lines, giving variation in the vertical direction, but no variation in the horizontal direction. Therefore the magnitude function is zero, except for $w_l = 0$. The magnitude image is that of situation A, but with a 90° rotation.

In situation C, the spatial image has horizontal and vertical lines, giving variation in both the vertical and horizontal directions. The spatial frequency image is a combination of that of situations A and B. There are nonzero magnitudes for $w_l = 0$ and for $w_n = 0$. If there had been slant lines in the spatial image, the magnitude values outside these two lines would also have been nonzero.

In situation D, there are more vertical than horizontal lines, giving more variation in horizontal direction than in vertical direction. Therefore, the magnitude image has more nonzero intensities for $w_l$ in the higher spatial frequencies.

The simple situation shown here gives a hint of how the magnitude images look in a complex situation. Examples of this are given in Figs. 4 and 9.

## REFERENCES

1 P. Geladi, K. Esbensen and S. Wold, Image analysis and chemical information in images, *Analytica Chimica Acta*, 191 (1986) 473–480.
2 P. Geladi and K. Esbensen, Can image analysis provide information useful in chemistry?, *Journal of Chemometrics*, 3 (1989) 419–429.
3 P. Trebbia and N. Bonnet, EELS elemental mapping with unconventional methods. I. Theoretical basis: analysis with multivariate statistics and entropy concepts, *Ultramicroscopy*, 34 (1990) 165–178.
4 P. Trebbia and C. Mory, EELS elemental mapping with unconventional methods. II. Applications to biological specimens, *Ultramicroscopy*, 34 (1990) 179–203.
5 G. Abousleman, R. Jordan and R. Griffey, Eigenvector-based spectral enhancement of nuclear magnetic resonance profiles of small volumes from human brain tissue, *Applied Spectroscopy*, 45 (1991) 202–208.
6 D. Bright and D. Newbury, Concentration histogram imaging. A scatter diagram technique for viewing two or three related images, *Analytical Chemistry*, 63 (1991) 243A–250A.
7 A. Eriksen and D. Cowan, Further development and application of GIS technology and geostatistics to assist in the exploration for uranium in western North America, *Proceedings of Remote Sensing for Exploration Geology, October 2–6, 1989, Calgary,* Environmental Research Institute of Michigan, Ann Arbor, MI, pp. 1285–1307.
8 P. Geladi, H. Isaksson, L. Lindqvist, S. Wold and K. Esbensen, Principal component analysis on multivariate images, *Chemometrics and Intelligent Laboratory Systems*, 5 (1989) 209–220.

9 K. Esbensen and P. Geladi, Strategy of multivariate image analysis (MIA), *Chemometrics and Intelligent Laboratory Systems*, 7 (1989) 67–86.
10 H. Grahn, N. Szeverenyi, M. Roggenbuck, F. Delaglio and P. Geladi, Data analysis of magnetic resonance images: 1. A principal component analysis approach, *Chemometrics and Intelligent Laboratory Systems*, 5 (1989) 311–322.
11 H. Grahn, N. Szeverenyi, M. Roggenbuck and P. Geladi, Tissue discrimination in magnetic resonance imaging: A predictive multivariate approach, *Chemometrics and Intelligent Laboratory Systems*, 7 (1989) 87–93.
12 P. Geladi and K. Esbensen, Multivariate image analysis in chemistry: an overview, in J. Devillers and W. Karcher (Editors), *Applied Multivariate Analysis in SAR and Environmental Studies*, Kluwer Academic Publishers, Dordrecht, 1991, pp. 415–445.
13 P. Geladi, H. Grahn and F. Lindgren, Chemical multivariate image analysis: some case studies, in J. Devillers and W. Karcher (Editors), *Applied Multivariate Analysis in SAR and Environmental Studies*, Kluwer Academic Publishers, Dordrecht, 1991, pp. 447–478.
14 K. Esbensen, M. Robb, G.-H. Strand and P. Geladi, Software review, *Chemometrics and Intelligent Laboratory Systems*, 5 (1988) 95–98.
15 P. Geladi and K. Esbensen, Regression on multivariate images: principal component regression for modeling, prediction and visual diagnostic tools, *Journal of Chemometrics*, 5 (1991) 97–111.
16 P. Geladi, E. Bengtsson, K. Esbensen and H. Grahn, Image analysis in chemistry. Part 1: Properties of images, greylevel operations, the multivariate image, *Trends in Analytical Chemistry*, 11 (1992) 41–53.
17 W. Pratt, *Digital Image Processing*, Wiley, New York, 1978.
18 H. Andrews, Two-dimensional transforms, in T. Huang (Editor), *Picture Processing and Digital Filtering*, Springer, Berlin, 1979.
19 P. Geladi, H. Grahn, K. Esbensen and E. Bengtsson, Image analysis in chemistry. Part 2: Operations on multivariate images, *Trends in Analytical Chemistry*, (1991) in press.
20 R. Brereton, Fourier transforms: use, theory and applications to spectroscopic and related data, *Chemometrics and Intelligent Laboratory Systems*, 1 (1986) 17–31.
21 R. Ramirez, *The FFT Fundamentals and Concepts*, Prentice-Hall, Englewood Cliffs, 1985.
22 A. Marshall (Editor), *Fourier, Hadamard and Hilbert Transforms in Chemistry*, Plenum Press, New York, 1982.
23 R. Gonzalez and P. Wintz, *Digital Image Processing*, Addison-Wesley, Reading, MA, 1977.
24 R. Bates and M. McDonnell, *Image Restoration and Reconstruction*, Clarendon Press, Oxford, 1986.